

Improved uncertainty quantification for Gaussian process regression based interatomic potentials

Albert P. Bartók^{1,2} and James R. Kermode²

¹*Department of Physics, University of Warwick, Coventry, CV4 7AL, United Kingdom*

²*Warwick Centre for Predictive Modelling, School of Engineering, University of Warwick, Coventry, CV4 7AL, United Kingdom*

(Dated: 20 June 2022)

The error estimation capability of machine learning interatomic potentials (MLIPs) based on probabilistic learning methods such as Gaussian process regression (GPR) is currently underexploited, because of the tendency of the predicted errors to overestimate the true error. We present approaches based on maximising either the marginal likelihood or an alternative likelihood constructed using leave-one-out cross validation to provide improved error estimates for interatomic potentials based on GPR. We benchmarked these approaches on models representing the Ar trimer, showing significant improvements in the robustness of the predicted error estimates.

I. INTRODUCTION

Multiscale materials modelling has been successful in many domains but it has not fully delivered on its promise, in large part because coupling of scales remains *ad hoc*, lacking the robust propagation of uncertainties across scales that is essential for reliable validated models. Most current research applies interatomic potential methods, despite severe limitations in accuracy and transferability. To date, there has been limited systematic analysis of the variation in simulation results with changes in the choice or parameters of the interatomic potential, mostly using “sloppy models” consisting of ensembles of potentials.^{1–3} These approaches are typically too costly to allow robust error bars to be placed on the outputs of complex simulations. Recently, alternative approaches based on calibrating “committees” of models, for example trained on subsets of the overall training data^{4,5} have seen some success, but so far lack the rigorous statistical underpinning needed for robust error propagation to derived quantities. The related “dropout” artificial neural network (ANN) approach has a Bayesian interpretation.⁶

The more challenging task of quantifying model form error requires sampling over ensembles of “reasonable” interatomic potentials that are not constrained by a predefined functional form, allowing them to better reflect the complexity of the underlying quantum mechanics. This is closely aligned to the broad body of recent literature that reports efforts to construct machine learning interatomic potential (MLIP)s that interpolate from a database of reference *ab initio* calculations, e.g. widely used artificial neural network⁷ and Gaussian approximate potentials (GAP)⁸ approaches, the spectral neighbour analysis potential (SNAP) method⁹ and related Linear Machine Learning (LML)¹⁰ approach, as well as the recently proposed atomic cluster expansion (ACE)¹¹ framework. Data-driven models avoid many of the pitfalls of a fixed functional form, but the errors induced by overly flexible models have not yet been systematically quantified. While MLIPs based on Gaussian process (GP)

regression are in principle accompanied by posterior variance estimates, this has been underexploited because of the tendency of GP predicted errors to overestimate the true uncertainty, combined with the high computational cost and complexity of optimising or sampling hyperparameters. For example, a recent GP-based potential for refractory high entropy alloys¹² was limited to two- and three-body terms only, and then also had to be remapped from GPs to splines for computational efficiency, removing the UQ capabilities (although a recent preprint addresses this by also mapping the error bars¹³).

While MLIPs are already extremely successful, for example, they have been applied to complex alloys with promising results,^{12,14} their uncertainty quantification (UQ) capabilities have severe limitations at present, with validation often being confined to test/train split rather than computing realistic quantities of interest (QoIs). Here, we present a step towards overcoming these limitations building on prior work from a number of research groups that demonstrates that MLIPs can be invested with UQ capabilities.^{4,5,7,8,15,16} We use a dataset consisting of Ar dimers and trimers computed at the CCSD(T) level to demonstrate the principles of our newly proposed approach.

II. METHODOLOGY

A. Data generation

We have generated a data set of 41 Ar dimers at interatomic distances uniformly spaced between 3 and 7 Å. In addition, a set of 1880 Ar trimers were generated by varying the bond distances between 3 and 7 Å and the bond angle between 0°–180°. We evaluated the *ab initio* energies with the Gaussian16 software package¹⁷ at the coupled cluster [CCSD(T)] level using the aug-cc-pVQZ basis set¹⁸. This ensures that dispersion interactions, which are largely responsible for attraction between the Ar atoms, are accurately modelled, including their many-body character. Consequently, the target interaction en-

ergy of an Ar trimer configuration is truly a function of all three atomic positions, and while the interaction is dominated by pair interactions, the total energy cannot be exactly decomposed into two-body terms.

B. Gaussian process regression

We can model any multivariate function $f(\mathbf{x})$ using a GP. This allows us to define a prior over functions that is equivalent to a multivariate normal distribution for any finite realisation of the function on a grid of N_* points $X_* = [\mathbf{x}_1, \mathbf{x}_2, \dots, \mathbf{x}_{N_*}]$ so that $\mathbf{f} = [f(\mathbf{x}_i), i = 1 \dots N_*]$, i.e.

$$f \sim \mathcal{GP}(m(\mathbf{x}), k(\mathbf{x}, \mathbf{x}')) \implies \mathbf{f} \sim \mathcal{N}(\mathbf{m}(\mathbf{x}), K) \quad (1)$$

where $m(\mathbf{x})$ is a specified mean function (often taken to be zero), $k(\mathbf{x}, \mathbf{x}')$ defines a kernel for the covariance between function values at input points \mathbf{x} and \mathbf{x}' and K is the resulting covariance matrix for all pairs of inputs, i.e. $K_{ij} = k(\mathbf{x}_i, \mathbf{x}_j)$ for $i, j = 1 \dots N$.

Consider a set of N noisy observations $\mathbf{y} = [y_1, y_2, \dots, y_N]$ at inputs $X = [\mathbf{x}_1, \mathbf{x}_2, \dots, \mathbf{x}_N]$ which are assumed to follow the model $f(\mathbf{x})$ on average but contaminated with additive Gaussian noise

$$y_i = f(\mathbf{x}_i) + \epsilon \text{ where } \epsilon \sim \mathcal{N}(0, \sigma_n^2) \quad (2)$$

where σ_n is a hyperparameter representing the noise level. Assuming additive independence, the covariance matrix for the observations is

$$\text{cov}[\mathbf{y}] = K_y = K(X, X) + \sigma_n^2 I \quad (3)$$

Conditioning the prior GP (1) on the data leads to a new GP representing our updated knowledge of the function, referred to as the posterior GP. The posterior GP can be used to compute the predictive mean and covariance at input points of interest X^* analytically¹⁹, with the results given by

$$\bar{\mathbf{f}}(X^*) = K(X_*, X)K_y^{-1}\mathbf{y} \quad (4)$$

$$\text{cov}[\mathbf{f}^*] = K(X_*, X_*) - K(X_*, X)K_y^{-1}K(X, X_*) \quad (5)$$

C. Gaussian approximation potentials

The GAP framework has been developed for the specific case of modelling an *ab initio* potential energy surface (PES) using Gaussian process regression (GPR)^{8,20}. In this framework, the GP inputs \mathbf{x} are computed using *descriptors* that are invariant to translation, permutation and rotational symmetries²¹, and the observations are the *ab initio* energies, and often also their derivatives in the form of forces and stresses. A complication arises here since we need to infer the decomposition of the total energy onto individual atoms (since local energies cannot be directly predicted with *ab initio* methods)

Consider first a two-body approximation to the total energy:

$$E(\mathbf{r}) = \sum_{i < j} V_2(r_{ij}) \quad (6)$$

where $V_2(r) \sim \mathcal{GP}(0, k_2(r, r'))$ and $r_{ij} = |\mathbf{r}_j - \mathbf{r}_i|$ is the distance between atoms i and j . Since we only have observations of the total energy, the target data is the sum of Gaussian Process models. The covariance between the total energies of two configurations A and B is simply the sum of the covariance functions for each bond

$$\langle E_A E_B \rangle = \sum_{ij \in A, i'j' \in B} k_2(r_{ij}, r_{i'j'}) \quad (7)$$

In the more general case the required covariances can be computed by introducing a linear operator \hat{L} which maps from the observations \mathbf{y} we have to the local atomic energies \mathbf{y}' through the relation $\mathbf{y} = \hat{L}^T \mathbf{y}'$. We refer the reader to Ref. 20 for a complete discussion of GPR in the context of interatomic potentials, which for realistic potentials also requires the use of a sparse GP to reduce the $O(N^3)$ cost of training; this step neglected here for simplicity.

In this work, we use a two-body potential which is a combination of explicit basis functions and a non-parametric term, and a fully non-parametric three-body potential. The total energy is of the form

$$E(\mathbf{r}) = E_0 + \sum_{i < j} V_2(r_{ij}) + \sum_{i < j < k} V_3(r_{ij}, r_{ik}, r_{jk}) \quad (8)$$

where E_0 is the average energy per atom across the training set. We note care must be taken to enforce permutation symmetry for the three-body term, either by symmetrising the descriptor or by summing the term over the permutation group of three particles; here, we take the former approach.

The elements of the symmetrised three-body descriptor $\mathbf{d} = [d_1, d_2, d_3]$ are defined as $d_1 = r_{ij} + r_{ik}$, $d_2 = (r_{ij} - r_{ik})^2$ and $d_3 = r_{jk}$, which ensures invariance to rigid rotations and translations as well as swapping the indices of j and k , while providing a bijective mapping between atomic coordinates and the descriptor elements.

D. Explicit basis functions

By analogy with the Kennedy–O'Hagan approach,²² simple models that encode known physics such as short-range repulsion can be used as a baseline; this has been explored already in GAP models in deterministic settings (e.g. to add van der Waals corrections²³) but the contributions made by uncertainty in the basis functions have not previously been included in predictions.

For the two- and three-body GPs, we use

$$V_2(r) = f_2(\mathbf{r}) + \mathbf{h}^T(r)\boldsymbol{\beta} \quad (9)$$

$$f_2(r) \sim \mathcal{GP}(0, k(r, r')) \quad (10)$$

$$V_3(\mathbf{r}) \sim \mathcal{GP}(0, k_3(\mathbf{r}, \mathbf{r}')) \quad (11)$$

This corresponds to the usual zero-mean GP for the three-body term, but a non-zero mean for the two-body term which is made up of a linear combination of basis functions $\mathbf{h}(r) = [h_1(r), h_2(r), \dots]$ with weights $\boldsymbol{\beta}$.

Following O’Hagan²⁴, if we adopt a Gaussian prior on the weights $\boldsymbol{\beta}$, so that $\boldsymbol{\beta} \sim \mathcal{N}(\mathbf{b}, B)$ we can integrate out the weights rather than optimising them. This yields another GP for $V_2(r)$

$$V_2(r) \sim \mathcal{GP}(\mathbf{h}(r)^T \mathbf{b}, k_2(r, r') + \mathbf{h}(r)^T B \mathbf{h}(r')) \quad (12)$$

Note that, while the mean of the new GP is simply equal to the product of the mean coefficients and the fixed basis functions, there is also a contribution to the covariance caused by the uncertainty in the coefficients. Taking the limit of an uninformative prior $B^{-1} \rightarrow 0$ gives results for the predictive mean and covariance which extend (4) and (5) to

$$\bar{V}_2(X_*) = \bar{\mathbf{f}}_2(X_*) + R^T \bar{\boldsymbol{\beta}} \quad (13)$$

$$\text{cov}[\mathbf{V}_2^*] = \text{cov}[\mathbf{f}_2^*] + R^T (H K_y^{-1} H^T)^{-1} R \quad (14)$$

where the design matrix $H = [\mathbf{h}(r_1), \mathbf{h}(r_2), \dots]$ collects the basis vectors for all training cases, and H^* the same for all test cases, $R = H_* - H K_y^{-1} K_*$ and the limiting $\bar{\boldsymbol{\beta}} = (H K_y^{-1} H^T)^{-1} K_y^{-1} \mathbf{y}$.

E. Basis functions and covariance kernels

It remains to specify the basis functions and covariance kernels selected in this study. Since atomic interactions in Ar are largely dominated by van der Waals dispersion, which is attractive, and repulsion due to the Pauli exclusion principle, we chose basis functions taken from the Lennard-Jones potential, i.e.

$$h_1(r) = \frac{1}{r^{12}} \quad (15)$$

$$h_2(r) = \frac{1}{r^6} \quad (16)$$

For both terms we chose squared-exponential (SE) covariance kernels of the forms

$$k_2(r, r') = \delta_2^2 \exp\left[\frac{|r - r'|^2}{\ell^2}\right] \quad (17)$$

$$k_3(\mathbf{d}, \mathbf{d}') = \delta_3^2 \exp\left[\sum_{i=1}^3 \frac{|d_i - d'_i|^2}{(\ell_3^i)^2}\right] \quad (18)$$

with the inputs r, \mathbf{r} and lengthscale hyperparameters $\theta_2, \boldsymbol{\theta}_3$ are scalars and three-vectors for the two-body and three-body case, respectively, and the signal variances δ_2 and δ_3 are both scalars, giving a total of 7 hyperparameters including the likelihood noise σ_n in (3), which we collect into a vector $\boldsymbol{\theta} = [\delta_2, \ell_2, \delta_3, \ell_3^1, \ell_3^2, \ell_3^3, \sigma_n]$. The cutoff distances for the two- and three-body terms were fixed at 7 Å and 5 Å, respectively.

F. Hyperparameter optimisation

For the Bayesian interpretation of a kernel model to be meaningful, attention must be paid to the choice of hyperparameters $\boldsymbol{\theta}$. Up until now these have often been set heuristically by MLIP practitioners for reasons of simplicity and computational expediency. In this work, kernel hyperparameters are optimised by maximising either the marginal likelihood (ML), which has previously been reported to improve predicted variances for GP-based interatomic potentials,^{15,16} and the leave-one-out cross validation (LOO-CV) likelihood, which has the advantage that it does not depend on the validity of modelling assumptions.

The marginal likelihood is the probability of the observed data given the inputs, and can be computed by integrating the likelihood multiplied by the prior (i.e. marginalising over the function values \mathbf{f}), leading to

$$p(\mathbf{y}|X, \boldsymbol{\theta}) = \int p(\mathbf{y}|\mathbf{f}, X, \boldsymbol{\theta}) p(\mathbf{f}|X, \boldsymbol{\theta}) d\mathbf{f} \quad (19)$$

For a zero mean GP the prior and likelihood are both Gaussian, so integral is analytic and yields

$$\log p(\mathbf{y}|X, \boldsymbol{\theta}) = -\frac{1}{2} \mathbf{y}^T K_y^{-1} \mathbf{y} - \frac{1}{2} \log |K_y| - \frac{N}{2} \log 2\pi, \quad (20)$$

which is simply the PDF of the observations $\mathbf{y} \sim \mathcal{N}(\mathbf{0}, K_y)$. The three terms can be interpreted as a data fit term, a complexity penalty and a normalisation constant, respectively. For the explicit basis in the limit of a non-informative prior on the basis coefficients $\boldsymbol{\beta}$ this result becomes

$$\log p(\mathbf{y}|X, \boldsymbol{\theta}) = -\frac{1}{2} \mathbf{y}^T K_y^{-1} \mathbf{y} + \frac{1}{2} \mathbf{y}^T C \mathbf{y} - \frac{1}{2} \log |A| - \frac{1}{2} \log |K_y| - \frac{N - M}{2} \log 2\pi \quad (21)$$

where $A = H K_y^{-1} H^T$, $C = K_y^{-1} H^T A^{-1} H K_y^{-1}$ and M is the rank of H^T .¹⁹

The LOO-CV approach is based on the idea of leaving out each piece of training data in turn. The predictive log probability of the data when leaving out training case i is

$$\log p(y_i|X, \mathbf{y}_{-i}, \boldsymbol{\theta}) = -\frac{1}{2} \log \sigma_i^2 - \frac{(y_i - \mu_i)^2}{2\sigma_i^2} - \frac{1}{2} \log 2\pi \quad (22)$$

where \mathbf{y}_{-i} means all observations except for number i , and the predictive mean μ_i and variance σ_i^2 are given by (13) and (14) using reduced training sets $\{X_{-i}, \mathbf{y}_{-i}\}$. From this result we can write down the LOO log predictive probability as

$$L_{LOO}(X, \mathbf{y}, \boldsymbol{\theta}) = \sum_{i=1}^N \log p(y_i|X, \mathbf{y}_{-i}, \boldsymbol{\theta}) \quad (23)$$

This can be computed efficiently by noting that we require a series of inverses of the full K_y , each with a row

and column deleted²⁵ which leads to simplified expressions for the LOO-CV predictive mean and variance of the form

$$\mu_i = y_i - [K_y^{-1}\mathbf{y}]_i/[K_y^{-1}]_{ii} \quad (24)$$

$$\sigma_i^2 = 1/[K_y^{-1}]_{ii} \quad (25)$$

Contributions from the explicit basis functions can be added in an analogous way. The LOO-CV likelihood can thus be computed with a computational cost that is dominated by a single inversion of K_y .

III. RESULTS

We used the CCSD(T) Ar dimer and trimer data to explore alternative strategies for choosing GP hyperparameters. To simulate the low-data limit, we trained our models on a fixed 1% subset of the data (19 structures), and retained the other 99% (1902 structures) for testing.

One dimensional sweeps for the three hyperparameters for the two-body kernel are shown in Fig. 1, along with the decomposition of the marginal likelihood into the terms in (21): data fit (first term), the contribution from the explicit basis set (second and third terms) and the complexity penalty (fourth term). The plot shows some differences in the maxima identified by the marginal likelihood and the LOO-CV likelihood, with the latter being more strongly peaked and for example preferring a smaller lengthscale and lower noise variance.

We next chose the hyperparameters using three approaches: (i) adopting the physically informed heuristic choices of hyperparameters commonly used when fitting GAP models; (ii) maximising the marginal likelihood of the training data; (iii) maximising the LOO-CV likelihood of the training data. In case (i) we first fitted a Lennard-Jones model to the training data and subtracted this from the CCSD(T) data before fitting the GAP model while in cases (ii) and (iii) we used the explicit basis function approach described above to fit the parametric and non-parametric terms together. Likelihoods were maximised using the BFGS algorithm, with derivatives with respect to hyperparameters computed using automatic differentiation²⁶. Multiple restarts with random initial choices for the hyperparameters were used to mitigate local maxima. We found that the best results are obtained with a single basis function $h_1(r)$ to account for short-range repulsion, without the long-range dispersion term $h_2(r)$. Table I summarises the hyperparameters obtained with each approach.

The results shown in Fig. 2 demonstrate that the ML approach has the highest accuracy on the training configurations, but the LOO-CV approach has the most reliable predicted errors. The GAP heuristics lead to predicted errors which are often significantly overestimate the true error (in accordance with previous observations²⁰). The ML predicted errors do have good correlation with true error (despite the overall high accuracy). The decomposition of the two-body energies is

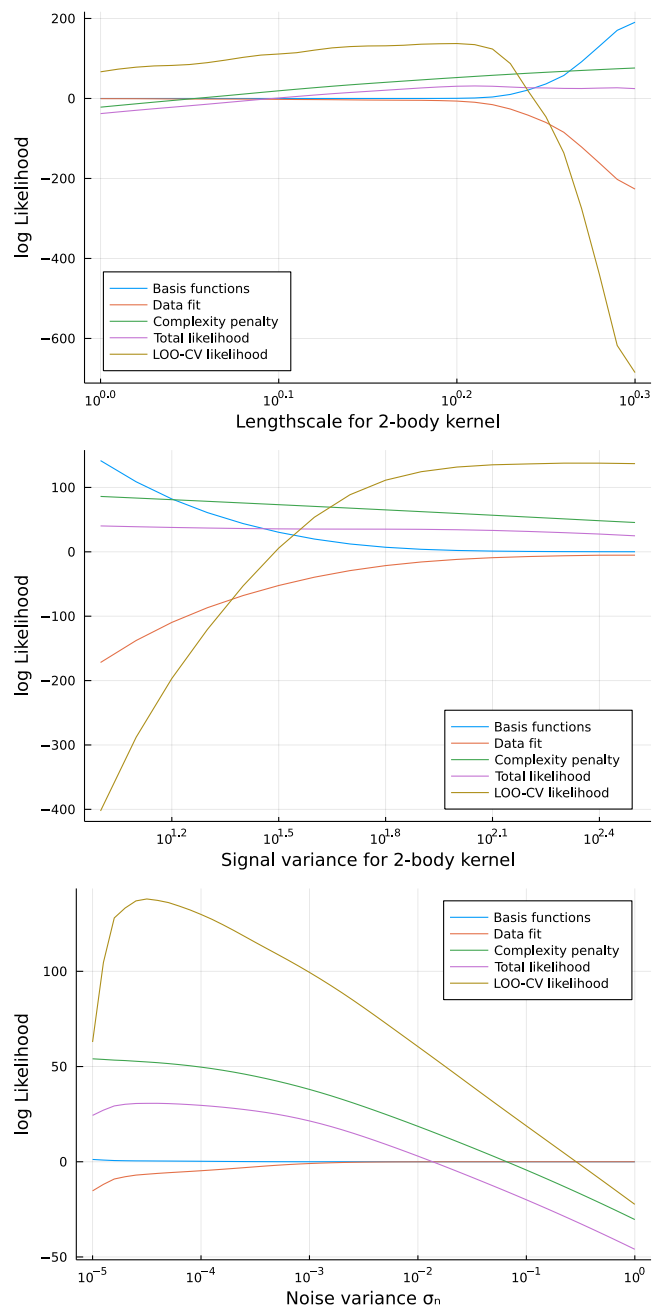


FIG. 1. Comparison of the ML and LOO-CV likelihood as a function of the three hyperparameter in the two-body kernel $k_2(r, r')$; from top to bottom, $\ell_2, \delta_2, \sigma_n$. The decomposition into the terms of (21) is also shown.

shown in Fig. 3. The explicit basis set makes a large contribution to the total uncertainty at distances beyond the cutoff of the non-parametric term; it is notable that this contribution is larger in the LOO-CV case.

The differences in performance can be rationalised by comparing the δ_2 and δ_3 values in Table 1. Recall that with a SE kernel the posterior predicted error, evaluated at a test point that is far from training data, tends to δ .

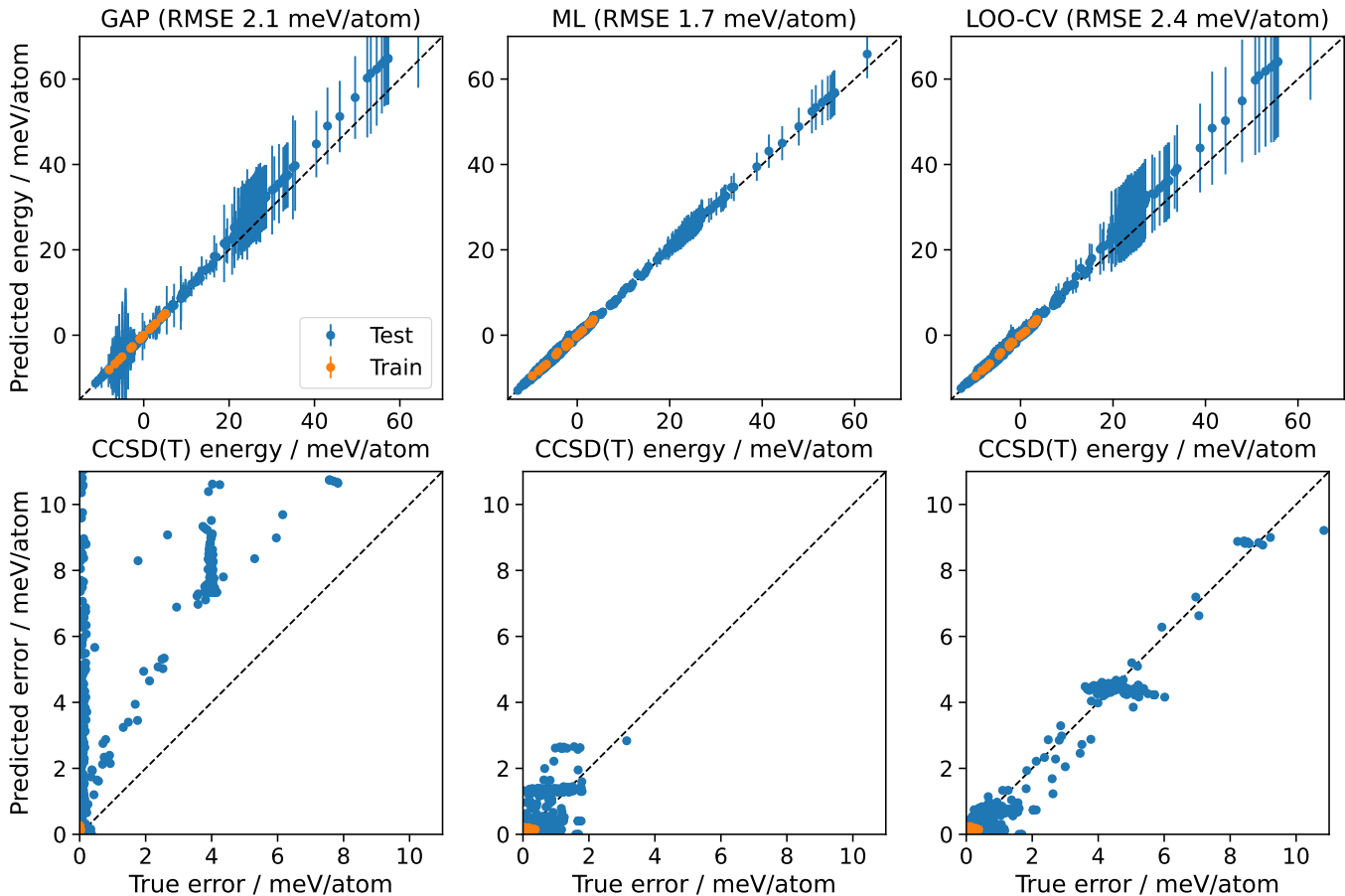


FIG. 2. GP models trained on quantum chemistry CCSD(T) calculations for Ar dimers and trimers, trained on 1% of the data (orange) and tested on remaining 99% (blue). Three realisations of the model, with hyperparameters chosen using heuristics as in GAP framework (left), optimised to maximise the marginal likelihood (ML, middle) or the LOO-CV (right). Note similar accuracy for the mean, but far superior predicted errors with LOO-CV, with GAP heuristics over-estimating and ML under-estimating true errors.

	GAP	Opt. ML	Opt. LOO-CV
Two-body			
δ_2 / eV	0.1	0.017	1429
$\ell_2 / \text{\AA}$	0.5	1.01	2.18
Three-body			
δ_3 / eV	0.05	0.0005	0.0006
$\ell_1 / \text{\AA}$	3.96	1054	239
$\ell_2 / \text{\AA}^2$	3.99	499	329
$\ell_3 / \text{\AA}$	6.50	917	344
σ_n / eV	0.001	0.00077	0.00077
RMSE / meV/atom	2.1	1.7	2.4

TABLE I. Hyperparameter values obtained with each of three approaches: GAP heuristics, optimising the marginal likelihood (ML) and optimising the LOO-CV likelihood. The final row in the table shows the RMSE of the resulting fits.

This is due to the variance in (5) dominated by the first term, as the second term tends to zero for very dissimilar pairs of configurations. The original GAP heuristics assign relatively similar weights to the two- and three-body

terms, while both optimised approaches put more weight on the two-body term, with the LOO-CV approach leading to an even greater two-body weighting. There are also significant differences in the lengthscales parameters, with LOO-CV leading to a more even split between the three components of the three-body descriptor than ML.

IV. CONCLUSIONS

Our results demonstrate that maximising the LOO-CV likelihood significantly improves the accuracy of the predicted errors over the marginal likelihood. To understand why this might be, recall that the marginal likelihood tells us the probability of the observations, given the assumptions of the model, while the LOO-CV likelihood gives an estimate for the predictive probability, whether or not the assumptions of the model are true, helping to make it more robust against model limitations²⁷.

Further work is required to extend this proof-of-principle to more complex manybody descriptors such

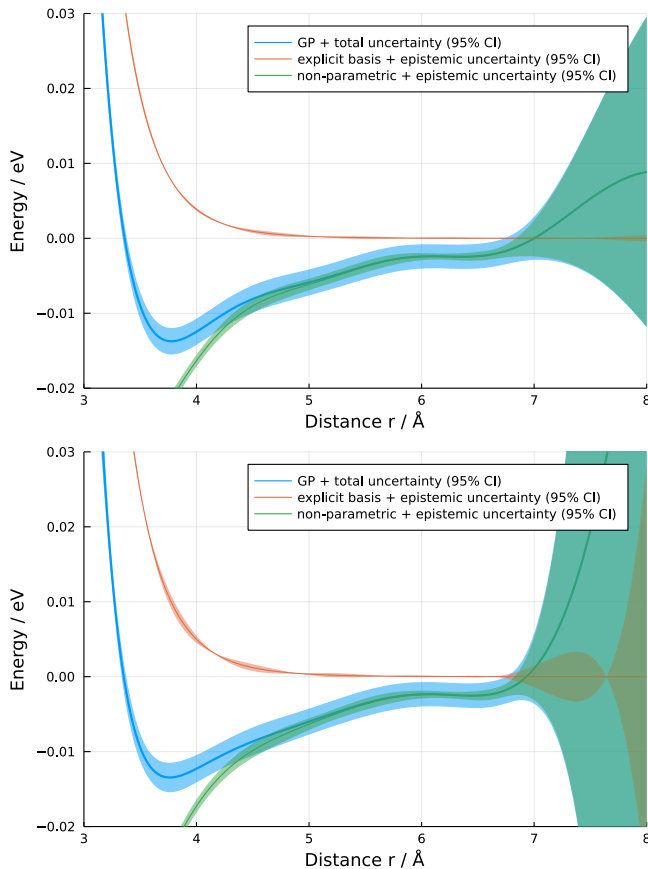


FIG. 3. Mean prediction and 95% confidence intervals for the 2-body component of the ML (above) and LOO-CV (below) models. Note large rise in predicted uncertainty beyond cutoff of 7 Å. Contributions from explicit polynomial basis and non-parametric regression are shown in red and green, respectively, with total prediction in blue.

as Smooth Overlap of Atomic Positions (SOAP)²¹ or ACE¹¹, and to the sparse GP case where, in principle, the set of inducing (sparse) points could also be optimised together with the hyperparameters. While the examples presented here used small training sets, LOO-CV approaches can be scaled to large datasets using Pareto-smoothed importance sampling,²⁸ giving scope to incorporate these ideas in production calculations.

ACKNOWLEDGMENTS

This work was financially supported by a Leverhulme Trust Research Project Grant (RPG-2017-191), the Engineering and Physical Science Research Council (EPSRC) under grant EP/R043612/1, the CASTEP-USER project funded by UK Research and Innovation under the grant agreement EP/W030438/1, and the NOMAD Centre of Excellence (European Commission grant agreement ID 951786). We acknowledge computational resources provided by the Scientific Computing Re-

search Technology Platform of the University of Warwick, STFC Scientific Computing Department’s SCARF cluster, the EPSRC-funded HPC Midlands+ consortium (EP/P020232/1, EP/T022108/1) and on ARCHER2 (<https://www.archer2.ac.uk/>) via the UK Car-Parinello consortium (EP/P022065/1). For the purpose of Open Access, the author has applied a CC-BY public copyright licence to any Author Accepted Manuscript (AAM) version arising from this submission.

- ¹S. L. Frederiksen, K. W. Jacobsen, K. S. Brown, and J. P. Sethna, “Bayesian ensemble approach to error estimation of interatomic potentials,” *Phys. Rev. Lett.* **93**, 165501 (2004).
- ²A. Mishra, S. Hong, P. Rajak, C. Sheng, K.-I. Nomura, R. K. Kalia, A. Nakano, and P. Vashishta, “Multiobjective genetic training and uncertainty quantification of reactive force fields,” *npj Comp. Mater.* **4**, 42 (2018).
- ³K. Tran, W. Neiswanger, J. Yoon, Q. Zhang, E. Xing, and Z. W. Ulissi, “Methods for comparing uncertainty quantifications for material property predictions,” *Mach. Learn.: Sci. Technol.* **1**, 025006 (2020).
- ⁴F. Musil, M. J. Willatt, M. A. Langovoy, and M. Ceriotti, “Fast and accurate uncertainty estimation in chemical machine learning,” *J. Chem. Theory Comput.* **15**, 906–915 (2019).
- ⁵G. Imbalzano, Y. Zhuang, V. Kapil, K. Rossi, E. A. Engel, F. Grasselli, and M. Ceriotti, “Uncertainty estimation for molecular dynamics and sampling,” *J. Chem. Phys.* **154**, 074102 (2021).
- ⁶M. Wen and E. B. Tadmor, “Uncertainty quantification in molecular simulations with dropout neural network potentials,” *npj Comp. Mater.* **6**, 1–10 (2020).
- ⁷J. Behler and M. Parrinello, “Generalized Neural-Network representation of High-Dimensional Potential-Energy surfaces,” *Phys. Rev. Lett.* **98**, 146401 (2007).
- ⁸A. P. Bartók, M. C. Payne, R. Kondor, and G. Csányi, “Gaussian approximation potentials: the accuracy of quantum mechanics, without the electrons,” *Phys. Rev. Lett.* **104**, 136403 (2010).
- ⁹A. P. Thompson, L. P. Swiler, C. R. Trott, S. M. Foiles, and G. J. Tucker, “Spectral neighbor analysis method for automated generation of quantum-accurate interatomic potentials,” *J. Comput. Phys.* **285**, 316–330 (2015).
- ¹⁰A. M. Goryaeva, J. Dérès, C. Lapointe, P. Grigorev, T. D. Swinburne, J. R. Kermode, L. Ventelon, J. Baima, and M.-C. Marinica, “Efficient and transferable machine learning potentials for the simulation of crystal defects in bcc Fe and W,” *Phys. Rev. Materials* **5**, 103803 (2021).
- ¹¹R. Drautz, “Atomic cluster expansion for accurate and transferable interatomic potentials,” *Phys. Rev. B* **99**, 014104 (2019).
- ¹²J. Byggmästar, K. Nordlund, and F. Djurabekova, “Modeling refractory high-entropy alloys with efficient machine-learned interatomic potentials: Defects and segregation,” *Phys. Rev. B* **104**, 104101 (2021).
- ¹³Y. Xie, J. Vandermause, S. Ramakers, N. H. Protik, A. Johansson, and B. Kozinsky, “Uncertainty-aware molecular dynamics from bayesian active learning: Phase transformations and thermal transport in SiC,” (2022), arXiv:2203.03824 [physics.comp-ph].
- ¹⁴C. W. Rosenbrock and et al., “Machine-learned interatomic potentials for alloys and alloy phase diagrams,” *npj Comp. Mater.* **7**, 1–9 (2021).
- ¹⁵J. Vandermause, S. B. Torrisi, S. Batzner, Y. Xie, L. Sun, A. M. Kolpak, and B. Kozinsky, “On-the-fly active learning of interpretable bayesian force fields for atomistic rare events,” *npj Comp. Mater.* **6**, 1–11 (2020).
- ¹⁶J. Vandermause, Y. Xie, J. S. Lim, C. J. Owen, and B. Kozinsky, “Active learning of reactive bayesian force fields: Application to heterogeneous hydrogen-platinum catalysis dynamics,” ArXiv:2106.01949 (2021), arXiv:2106.01949 [cond-mat.mtrl-sci].
- ¹⁷M. J. Frisch, G. W. Trucks, H. B. Schlegel, G. E. Scuseria, M. A. Robb, J. R. Cheeseman, G. Scalmani, V. Barone, G. A. Peters-

- son, H. Nakatsuji, X. Li, M. Caricato, A. V. Marenich, J. Bloino, B. G. Janesko, R. Gomperts, B. Mennucci, H. P. Hratchian, J. V. Ortiz, A. F. Izmaylov, J. L. Sonnenberg, D. Williams-Young, F. Ding, F. Lipparini, F. Egidi, J. Goings, B. Peng, A. Petrone, T. Henderson, D. Ranasinghe, V. G. Zakrzewski, J. Gao, N. Rega, G. Zheng, W. Liang, M. Hada, M. Ehara, K. Toyota, R. Fukuda, J. Hasegawa, M. Ishida, T. Nakajima, Y. Honda, O. Kitao, H. Nakai, T. Vreven, K. Throssell, J. A. Montgomery, Jr., J. E. Peralta, F. Ogliaro, M. J. Bearpark, J. J. Heyd, E. N. Brothers, K. N. Kudin, V. N. Staroverov, T. A. Keith, R. Kobayashi, J. Normand, K. Raghavachari, A. P. Rendell, J. C. Burant, S. S. Iyengar, J. Tomasi, M. Cossi, J. M. Millam, M. Klene, C. Adamo, R. Cammi, J. W. Ochterski, R. L. Martin, K. Morokuma, O. Farkas, J. B. Foresman, and D. J. Fox, "Gaussian 16 Revision C.01," (2016), gaussian Inc. Wallingford CT.
- ¹⁸D. E. Woon and T. H. Dunning, "Gaussian basis sets for use in correlated molecular calculations. iii. the atoms aluminum through argon," *J. Chem. Phys.* **98**, 1358–1371 (1993).
- ¹⁹C. E. Rasmussen and C. K. I. Williams, *Gaussian processes for machine learning*, Vol. 14 (MIT Press, 2006).
- ²⁰V. L. Deringer, A. P. Bartók, N. Bernstein, D. M. Wilkins, M. Ceriotti, and G. Csányi, "Gaussian process regression for materials and molecules," *Chem. Rev.* **121**, 10073–10141 (2021).
- ²¹A. P. Bartók, R. Kondor, and G. Csányi, "On representing chemical environments," *Phys. Rev. B* **87**, 184115 (2013).
- ²²M. C. Kennedy and A. O'Hagan, "Bayesian calibration of computer models," *J. R. Stat. Soc. Series B Stat. Methodol.* **63**, 425–464 (2001).
- ²³P. Rowe, V. L. Deringer, P. Gasparotto, G. Csányi, and A. Michaelides, "An accurate and transferable machine learning potential for carbon," *J. Chem. Phys.* **153**, 034702 (2020).
- ²⁴A. O'Hagan, "Curve fitting and optimal design for prediction," *J. R. Stat. Soc.* **40**, 1–24 (1978).
- ²⁵S. Sundararajan and S. S. Keerthi, "Predictive approaches for choosing hyperparameters in gaussian processes," *Neural Comput.* **13**, 1103–1118 (2001).
- ²⁶J. Revels, M. Lubin, and T. Papamarkou, "Forward-mode automatic differentiation in Julia," arXiv:1607.07892 [cs.MS] (2016).
- ²⁷G. Wahba, *Spline Models for Observational Data* (SIAM, 1990).
- ²⁸A. Vehtari, A. Gelman, and J. Gabry, "Practical Bayesian model evaluation using leave-one-out cross-validation and WAIC," *Stat. Comput.* **27**, 1413–1432 (2017).